AIChE

Cetyltrimethylammonium Bromide-Coated Agrosorbents and Their High Benzene Adsorption Performance from Aqueous Solution

Helen Kong,[a] Siew Chin Cheu,[a] Nurul Sakinah Othman,[b] Shiow Tien Song,[a] Khairiraihanna Johari,[c] Norasikin Saman,[a] Jimmy Wei Ping Lye,[a] and Hanapi Mat [a,d]

[a]Advanced Materials and Process Engineering Laboratory, Faculty of Chemical and Energy Engineering, Universiti Teknologi Malaysia, UTM Skudai, Johor 81310, Malaysia; hbmat@cheme.utm.my (for correspondence)

[b]Department of Chemical Engineering, School of Science and Engineering, Manipal International University (MIU), Nilai, Negeri Sembilan 71800, Malaysia

[c]Department of Chemical Engineering, Faculty of Engineering, Universiti Teknologi PETRONAS, Bandar Seri Iskandar, Perak 32610, Malaysia

[d]Advanced Materials and Separation Technologies (AMSET) Research Group, Health and Wellness Research Alliance, Universiti Teknologi Malaysia, UTM Skudai, Johor 81310, Malaysia

Published online 6 July 2017 in Wiley Online Library (wileyonlinelibrary.com). DOI 10.1002/ep.12678

Cetyltrimethylammonium bromide-coated agrosorbents were successfully synthesized through firstly mercerization of raw banana trunk (Raw-BT) with alkali (M-BT) and finally coating with cetyltrimethylammonium bromide (M-CTAB-BT). The characterization was done using an energy dispersive X-ray spectrophotometer, a Fourier transform infrared spectrophotometer and a field emission scanning electron microscope. The Brunauer, Emmett, and Teller analysis was also conducted. The benzene adsorption performance of BT agrosorbents was improved by mercerization and surfactant coating according to the following order: Raw-BT (340.25 × 10⁻ mmol/g) < CTAB-BT (382.41 × 10^{-3} mmol/g) < M-CTAB-BT (535.62 × 10^{-3} mmol/g). The adsorption data obeyed the Langmuir and pseudo-second order (PSO) kinetic models with film diffusion as the rate-limiting step. The agrosorbent regeneration as well as comparison to literature data indicated the modified BT and thus the agrowaste biomass could be alternative agrosorbent precursors for removing benzene from aqueous solutions. © 2017 American Institute of Chemical Engineers Environ Prog, 37: 305–317, 2018

Keywords: agrowaste, mercerization, surfactant, benzene, adsorption

Introduction

Benzene is one of the volatile organic compounds (VOC) which is highly flammable, toxic and carcinogenic [1,2]. It is generally used as either a raw material or a solvent in chemical and petrochemical related industries [3–7]. It is soluble in water and commonly found in the petroleum refinery effluent [8]. Benzene can enter the natural water bodies via leakage of the underground gasoline storage tanks and unintended oil spills [9]. The presence of benzene in the surface and ground water even at very low concentration can cause a severe impact on the environment and threaten the public health [5,10,11]. The World Health Organization (WHO) has governed that the maximum allowable benzene content in the drinking water to be 0.01 ppm [3], while the United States Environmental Protection Agency (US EPA) has also regulated the maximum benzene contaminant level as 0.005 ppm [12].

Due to the acute effect caused by benzene, the benzene removal from the various water bodies is utmost needed to ensure the safety of the environment. Among the available technologies, adsorption offers several advantages such as simple design and operation, lower energy requirement and cheaper operating costs [13–19]. Activated carbon has been the most widely employed adsorbent for benzene removal process due its high specific surface area and stability [4,10,20,21]. However, the strong binding between the benzene molecules and carbon surface has made it difficult for regeneration and thus increased the material and operating cost [22,23]. Besides, carbon nanotubes [24–26], zeolites [27,28], clays [12,29–31], macroreticular resins [32], diatomite [5,33], carbon–silica aerogel composites [34], and membranes [35–37] have been used as adsorbents for the removal of benzene and other VOCs. Every adsorbent material has its own advantages and drawbacks as benzene adsorbents. For instance, carbon nanotubes and membranes show the most promising benzene adsorption performance. However, they are more expensive than the conventional adsorbents [35,38]. Clay and zeolite materials are usually hydrophilic in nature, which are not beneficial for the benzene adsorption process. Various adsorbent modifications have been conducted to enhance the benzene adsorption uptake [12,39,40].

Additional Supporting Information may be found in the online version of this article.

Recently, various agrowastes have favorably been used as precursors to synthesize low-cost agrosorbents due to the fact that agrowaste is natural, abundant, low-priced, renewable and biodegradable. The applications of raw/unmodified agrowastes, such as rice bran, angico saw-dust, and peat as agrosorbents for BTEX removal were reported [41–43]. However, the use of unmodified agrowastes has found to have low adsorption capacity and selectivity [44,45]. Agrowastes especially the plant residues contain large amounts of hydroxyl groups which can be easily modified or functionalized with various functional groups to enhance their adsorption affinity towards specific pollutants [46,47]. The application of thermal treatment to modify agrowastes such as *Moringa oleifera* pods, coconut shell, peach stone, date pit, almond shell, and olive stone to produce activated carbon for BTEX removal from aqueous solution was reported [17,22,48]. Apart from the thermal treatment, the alkaline treatment known as a mercerization process helped increase the formation of carboxyl groups on the agrosorbent surfaces creating more possible binding sites [49]. The surface mercerization process enhances the binding effects by increasing surface roughness [45]. Moreover, the surface mercerization process would also improve the agrosorbent pore size by degrading the lignin in the agrowaste during the modification process [50].

Other chemical modifications such as esterification, acetylation, sulfonation, etherification, impregnation, and graft polymerization are commonly conducted [11,51–55]. Thus, different functional groups can be introduced on the agrosorbent surfaces to enhance the adsorptive affinity towards target adsorbates. For example, the surface modification by introducing various types of surfactants on the agrosorbent surfaces is one of the conventional methods to enhance the agrosorbent hydrophobicity [56]. Agrosorbents (e.g., wheat straw, barley straw, coconut coir pith, peanut husk, and yeast) modification by various cationic surfactants with different molecular weights such as cetyltrimethylammonium bromide (CTAB), cetylpyridinium bromide (CPB), cetylpyridinium chloride (CPC), hexadecyltrimethylammonium (HDTMA) were reported for removal of metal ions, dyes and oil from aqueous solutions [45,57–61]. Inorganic adsorbents such as clay and zeolite modified with cationic surfactants including HDTMA, benzyldimethyltetradecylammonium (BDTDA), benzyltrimethylammonium (BTMA) and CPB [28,30,62] were also used successfully. For instance, the cationic surfactant modified clay can remove benzene up to 70% of those shown by activated carbon [62]. However, there are no available data for the benzene adsorptive removal by cationic surfactants such as CTAB coated onto agrosorbents. The detailed analysis of benzene removal by a nonionic surfactant [i.e., 4-(1,1,3,3-tetramethylbutyl)phenyl-polyethylene glycol (Triton X-100)] modified agrosorbent was previously reported [63].

Therefore, in this study, the CTAB coated agrosorbents of banana trunk (BT) were synthesized, characterized, and applied for benzene removal from aqueous solution. The agrosorbents were prepared by first mercerizing the raw banana trunk (Raw-BT) using concentrated sodium hydroxide (NaOH) solution (M-BT) followed by coating with CTAB (M-CTAB-BT). Besides that, the nonmercerized BT coated with CTAB (CTAB-BT) was also synthesized. The equilibrium and kinetics of CTAB adsorption onto raw banana trunk (Raw-BT) and mercerized BT (M-BT) were investigated. The synthesized agrosorbents were characterized by using various analytical techniques. The performance of synthesized agrosorbents was evaluated for benzene adsorption from aqueous solution at various experimental conditions. The benzene adsorption data were examined by both equilibrium and kinetic models to study the adsorption mechanism. The findings of the present study were compared with the literature data to demonstrate the prospect of the agrowastes especially banana trunk as precursors for the low-cost agrosorbent synthesis for the benzene removal process from water and wastewater.

MATERIALS AND METHODS

Reagents

Cetyltrimethylammonium bromide (CTAB), chloroform, ethanol, isooctane, methanol, and sodium hydroxide (NaOH pellets) were purchased from Merck (Germany). Analytical grade benzene was obtained from Fisher Scientific (UK). Sodium dodecyl sulphate (SDS) was bought from Fluka (Switzerland). Double-distilled water was freshly prepared in the laboratory. The banana trunk (BT) was obtained from the nearby residential area.

Agrosorbents Preparation

The physical modification of the BT was carried out according to the previous study [63]. Agrosorbent surface mercerization was conducted by immersing 5 g of Raw-BT into 200 mL of 30% (w/v) sodium hydroxide (NaOH) aqueous solution. The mixture was agitated for 1 h under ambient condition. The sample was then washed with plenty of double-distilled water and filtered. The washed alkaline sample was dehydrated overnight at (50 ± 1)°C. The end product was denoted as M-BT.

CTAB aqueous solution of a desired concentration was prepared by dissolving an accurate quantity of CTAB powder in double-distilled water. The chemical modification was conducted by soaking an accurate amount of BT sample (i.e., Raw-BT or M-BT) into the CTAB solution. The mixture was stirred by a magnetic stirrer for 2 h, which was sufficient to reach equilibrium conditions. The sample was then repeatedly rinsed with double-distilled water to remove of unbounded CTAB from the agrosorbent surface. The sample was dehydrated at (50 ± 1)°C overnight. The CTAB modified Raw-BT and M-BT were respectively designated as CTAB-BT and M-CTAB-BT and kept in a desiccator. The CTAB loading capacity, Γ_e (mmol/g) of CTAB modified BT was calculated by (1)):

$$\Gamma_e = \frac{(C_0 - C_e) \cdot V_L}{m} \quad (1)$$

where C_0 and C_e are the initial and equilibrium CTAB concentration (mmol/L) respectively, V_L is the liquid phase volume (L), and m is the agrosorbent mass (g).

The CTAB concentration was determined by a colorimetric two-phase titration with SDS solution as a titrant in which a standard calibration curve of SDS solution volume against CTAB concentrations was constructed [64]. Typically, 5 mL of CTAB solution was pipetted into a conical flask (50 mL). It was then followed by adding 5 mL of each chloroform and double-distilled water in the flask, accordingly. 2 mL of acid mixed indicator was added into the mixture. The mixture was shaken and titrated with 0.004 mmol/L SDS solution. The colorless chloroform turned blue at the end point.

Agrosorbent Characterization

The elemental composition of respective agrosorbents was determined by an energy dispersive X-ray analysis (EDX) using Hitachi FEI Quanta 200F (Japan). A field emission scanning electron microscope (FESEM), model Hitachi S4800 (Japan), was employed to determine the agrosorbent surface morphology. The Brunauer, Emmett, and Teller (BET) pore size and surface area of agrosorbents were determined by the nitrogen adsorption/desorption method at −195.9°C (77.3 K), using Micromeritics ASAP 2000 (USA).

Table 1. Elemental analysis results of agrosorbents.

	Elemental composition (wt %)		
Elements	**Raw-BT**	**M-BT**	**M-CTAB-BT**
C	41.26	15.91	80.47
O	57.37	50.63	14.28
Na	0.64	32.91	0.11
Si	0.35	0.39	0.25
Br	0.38	0.15	4.87

The Fourier transform infrared spectroscopy (FTIR), model Thermo Fisher Scientific Nicolet, model iS5 (USA) equipped with attenuated total reflectance (ATR) sampling technique with OMNIC operating system (Version 7.0, Thermo Nicolet, USA) was used to determine the agrosorbent surface functional groups.

Benzene Adsorption

A high benzene concentration stock solution was prepared by dissolving an accurately weighed amount of analytical grade benzene (99% purity) in methanol (HPLC grade) [65]. The benzene solution at the desired concentration was freshly prepared by spiking the stock solution using a microsyringe into a volumetric flask filled with double-distilled water. A set of Erlenmeyer flasks (50 mL) with glass stoppers was used to carry out the adsorption experiments. An agrosorbent dosage of 0.5 mg/mL was employed. The mixture was agitated at 200 rpm for 24 h, which was adequate to achieve equilibrium, in a temperature-controlled shaker. The mixture supernatant was then sampled. The residual benzene in the supernatant was concentrated by using isooctane. An UV–VIS spectrophotometer model PerkinElmer Lambda 35 (USA) was used to determine the residual benzene concentration in the isooctane at λ_{max} = 255 nm [63]. The benzene adsorption capacity at any time t, q_t was also calculated using Equation (2) in which the C_e is however equal to C_t; the concentration at time t.

$$q_t = \frac{(C_0 - C_t) \cdot V}{W} \tag{2}$$

where C_0 is the initial benzene concentration (mmol/L), C_t is the residual benzene concentration at time t (mmol/L), V is the benzene solution volume (L), and W is the agrosorbent mass (g). The benzene adsorption capacity, q_t (mmol/g) at equilibrium is given as q_e (mmol/g).

The benzene adsorption experiments were carried out in a single run except for the data points that deviated significantly from the overall trend were repeated to ensure reproducibility of the results. A triplicate of the benzene concentration measurements was carried out and their average value was presented. The validity of equilibrium and kinetic models to the adsorption data was examined using the linear determination coefficient, R^2, the normalized standard deviation analysis, $\Delta\Gamma_e$ or Δq_e (%) and the Pearson's chi-squared test, χ^2 [63]. The experimental adsorption data were analyzed by adsorption isotherm and kinetic models to draw a thorough understanding on adsorption mechanism.

Results and discussion

Agrosorbent Characterizations

Table 1 displays the elemental composition of Raw-BT, M-BT, and M-CTAB-BT in which the M-BT had the highest content of sodium (32.91%) due to the formation of sodium counter-ion after reacting with 30% (w/v) NaOH solution.

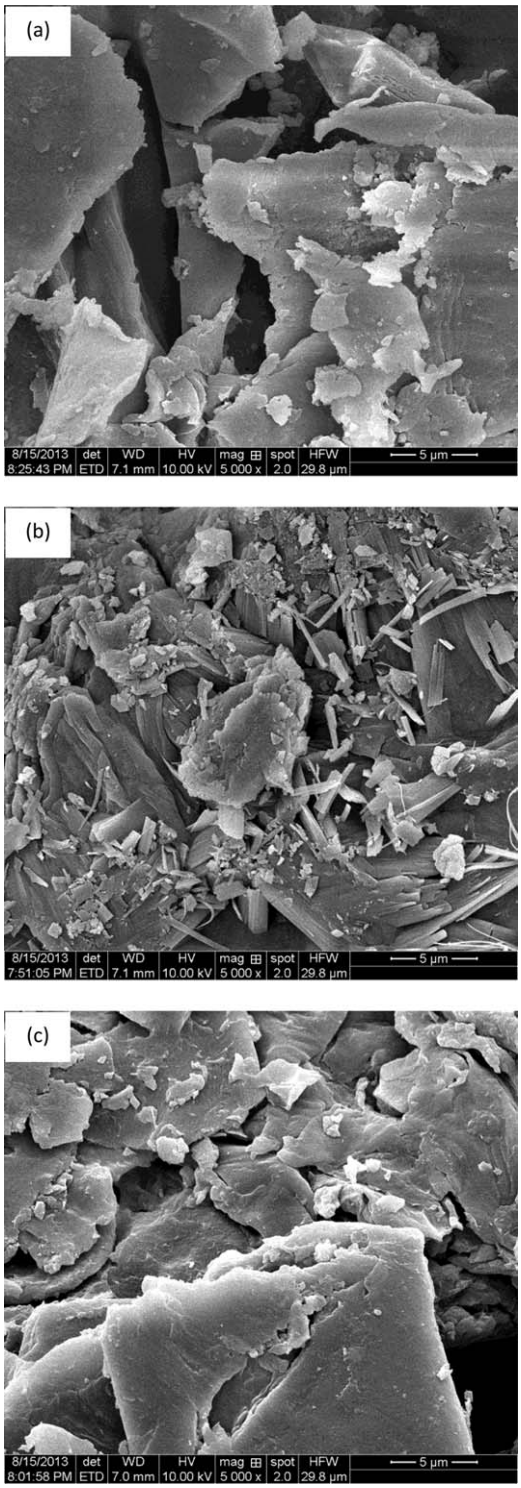

Figure 1. FESEM image of (a) Raw-BT, (b) M-BT, and (c) M-CTAB-BT.

The M-CTAB-BT has the highest content of carbon (80.47%) due to the introduction of the CTAB long alkyl tail to M-BT surfaces. Figure 1 shows FESEM image of (a) Raw-BT, (b) M-BT, and (c) M-CTAB-BT. The Raw-BT had a smooth and compact surface morphology (Figure 1a) however the M-BT indicated an uneven surface (Figure 1b). The rough surface of M-BT might be attributed to the mercerization treatment in which the smooth Raw-BT surfaces were destroyed. The M-CTAB-BT displayed a homogeneous and smoother surface

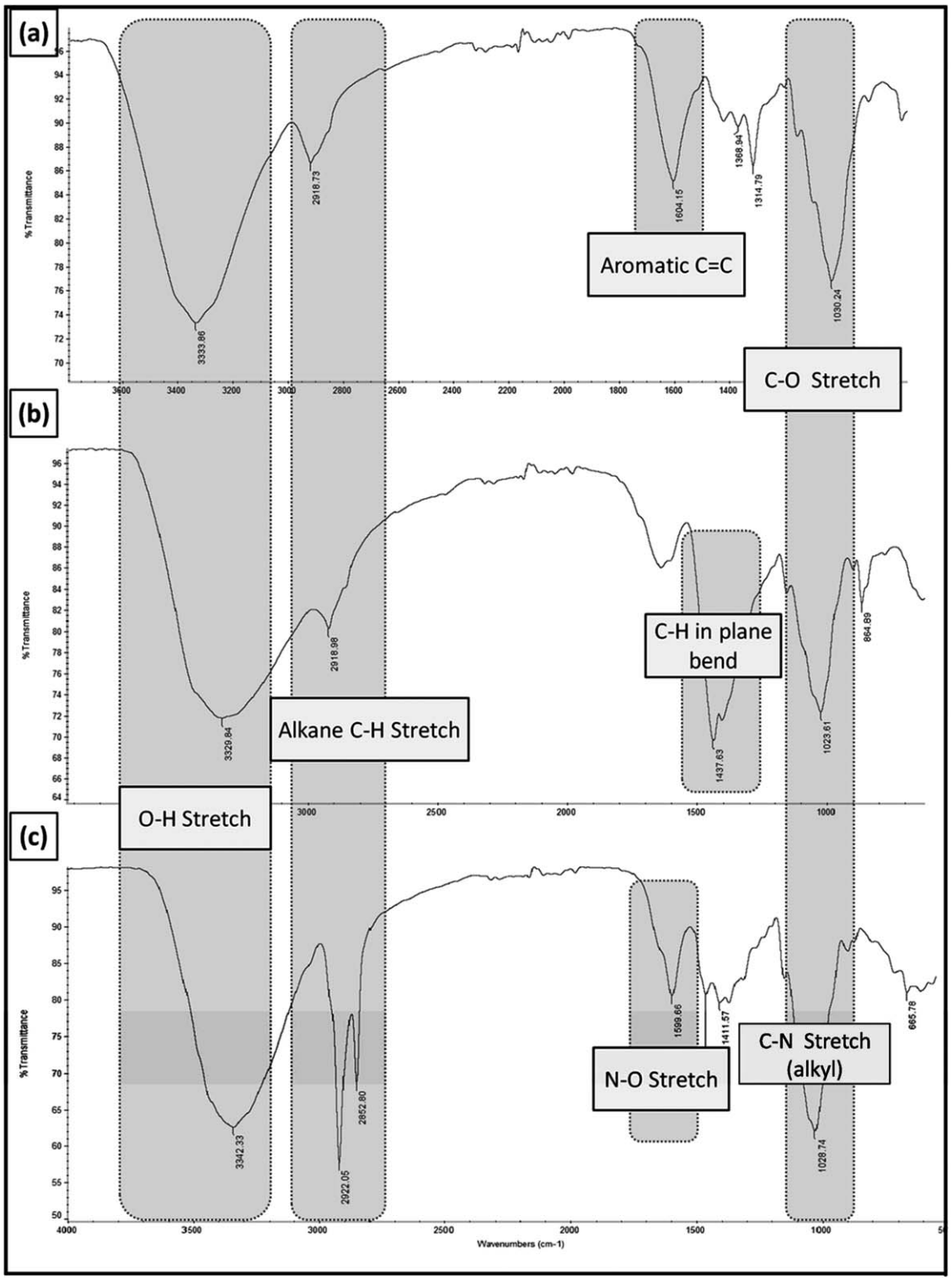

Figure 2. FTIR spectrum of (a) Raw-BT, (b) M-BT, and (c) M-CTAB-BT.

morphology in comparison to M-BT (Figure 1c). The M-CTAB-BT had the lowest surface area (0.834 m^2/g) and pore diameter (4.081 nm). This was followed by the CTAB-BT (surface area: 2.400 m^2/g; pore diameter: 10.440 nm). The low surface area and pore diameter obtained due to the occupancy by the lengthy CTAB alkyl structure on the agrosorbent surface [23]. On the contrary, the Raw-BT had the highest surface area (2.247 m^2/g) and pore diameter (10.970 nm). Figure 2 displays the FTIR spectra of the Raw-BT, M-BT, and M-CTAB-BT. Table 2 shows FTIR spectra of functional groups present in the respective agrosorbents. Figure 2a shows that the Raw-BT had the characteristic peaks at (3400–3300, 2950–2800, 1430–1290, 1368, 1600, and 1030) cm^{-1}. After the alkali treatment with concentrated NaOH solution, C═C stretching (aromatics) of M-BT was destroyed, however the alkene C—H bend was present at 1437 cm^{-1} (Figure 2b). Figure 2c shows that M-CTAB-BT had the two most recognizable peaks at approximately 2852

Table 2. The FTIR wavenumber (cm^{-1}) of various functional groups.

Functional groups	Molecular motion	Wavenumber (cm^{-1})
Alkanes	C—H stretching	2950–2800
	CH_2 bending	~1465
	CH_3 bending	~1375
Alkenes	C—H in plane bending	1430–1290
Alkynes	Acetylenic C—H bending	650–600
Aromatics	C=C stretching	~1600
	C—H bending (meta)	~880
	C—H bending (para)	850–800
Alcohols	O—H stretching	3400–3300
Aldehydes	C—H aldehyde stretching	~2850
Amines	N—H stretching	3500–3300
	C—N stretching (alkyl)	1200–1025
Nitro	N—O (aliphatic)	1600–1530
Sulfoxides	S=O stretching	~1050

Table 3. Benzene adsorption capacity of agrosorbents. Experimental conditions: benzene concentration, 1.0 mmol/L; contact time, 24 h; pH, 7; temperature (30 ± 1)°C; and dosage, 0.5 mg/mL.

Agrosorbents	Adsorption capacity, q_e ($\times 10^3$ mmol/g)
Raw-BT	33.538
M-BT	60.420
CTAB-BT	136.329
M-CTAB-BT	309.140

and 1600 cm^{-1} which indicated the existence of alkane C—H stretch and N—O stretching respectively after CTAB modification. Furthermore, Figure 2c also shows a sharper and narrower peak at 1028.74 cm^{-1} in comparison with Figure 2b. This indicated C—N stretching of the tertiary amine groups from the impregnated CTAB on the agrosorbent surfaces. The benzene adsorption capacity of the four synthesized agrosorbents is given in Table 3. It was found that the M-CTAB-BT had higher q_e as compared to CTAB-BT which might be attributed to higher CTAB loading capacity of the pretreated agrosorbent (i.e., M-BT).

Surfactant Adsorption Characteristics

Figure 3 displays the relationship between contact time and CTAB adsorption onto both Raw-BT and M-BT. Generally, the CTAB adsorption displays a rapid rate at the first few minutes for both agrosorbents. This phenomenon was observed because the large number of vacant sites on the fine agrosorbent particles which had higher probability to adsorb CTAB molecules. It was found that Γ_e (mmol/g) of M-BT increased with the initial CTAB concentrations and achieved equilibrium after 10 min. The data were analyzed by fitting to three well-known kinetic models (reaction-based) namely the pseudo-first order (PFO), pseudo-second order (PSO), and Elovich models (see Supporting Information SI 1) [66,67]. The calculated kinetic model parameters are presented in Table 4. It was found that both Raw-BT and M-BT kinetic data were best fitted by the PSO kinetic model since the highest R^2 value was obtained. The $\Delta\Gamma_e$ and χ^2 values of the PSO model for both Raw-BT and M-BT were also smaller in comparison with other models. Moreover, the Γ_{cal} (mmol/g) of the PSO model were approximately similar to $\Gamma_{t,\ exp}$ (mmol/g). The CTAB adsorption onto the M-BT had higher k_2 (14.437 min^{-1}) indicating that the M-BT had a higher CTAB adsorption rate compared to the Raw-BT (5.790 min^{-1}). The nonlinear PSO model fittings of the CTAB adsorption data for both Raw-BT and M-BT are given in Figure 4. The fitting result of other models is shown in Supporting Information (SI 3).

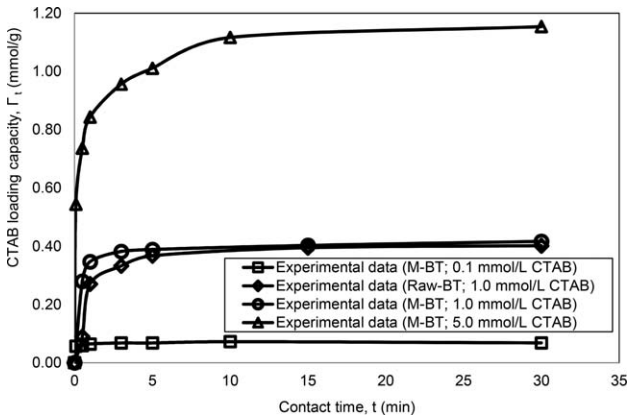

Figure 3. Effect of contact time on CTAB loading capacity at various CTAB concentrations. Experimental conditions: CTAB concentration, 0.1, 1.0, and 5.0 mmol/L; pH, 7; temperature (30 ± 1)°C; and dosage, 2 mg/mL.

The effects of initial CTAB concentrations on CTAB adsorption of the BT agrosorbents are given in Figure 5a. The Raw-BT and M-BT achieved its maximum loading capacity respectively after approximately 5 mmol/L. The M-BT achieved a higher q_e in comparison with the Raw-BT due to the pretreatment of the Raw-BT with 30% (w/v) NaOH resulted in destructured Raw-BT surfaces. Moreover, the pretreatment with alkali solution contributed to the formation of carboxyl groups on the BT surfaces and thus enhanced the CTAB adsorption (binding) effect [67]. The CTAB loading capacity data were examined by the Langmuir, Freundlich, Temkin, and Dubinin–Raduchkevich (D–R) isotherm models (Supporting Information SI 2). The generated parameters of the isotherm models are tabulated in Table 5. The experimental data for both Raw-BT and M-BT were best fitted by the Langmuir model based on R^2 of the Raw-BT (0.992), and M-BT (0.997) agrosorbents, respectively. The $\Delta\Gamma_e$ and χ^2 values of the Langmuir model for both Raw-BT and M-BT were also the smallest in comparison with other models. In addition, the $\Gamma_{max,L}$ (mmol/g) values obtained from the Langmuir isotherm model were reasonably closer to the $\Gamma_{e,\ max,\ exp}$ (mmol/g). Figure 5b shows the experimental data were well expressed by the non-linear Langmuir model fitting. The fitting result of other models is given in Supporting Information (SI 4). All these indicators described above had proved

Table 4. Kinetic model parameters obtained from CTAB loading rate analysis.

Samples Parameters	Raw-BT	M-BT
$\Gamma_{t,exp}$ (mmol/g)	0.402	0.417
Pseudo-first order (PFO)		
Γ_{cal} (mmol/g)	0.230	0.140
k_1 (min^{-1})	0.311	0.322
R^2	0.964	0.890
$\Delta\Gamma_e$ (%)	56.847	72.603
χ^2	1.309	4.134
Pseudo-second order (PSO)		
Γ_{cal} (mmol/g)	0.405	0.410
k_2 (min^{-1})	5.790	14.437
R^2	0.997	0.999
$\Delta\Gamma_e$ (%)	23.888	22.716
χ^2	0.004	0.001
Elovich		
β (g/mmol)	9.434	10.526
α (mmol/g.min)	0.475	0.805
R^2	0.572	0.400
$\Delta\Gamma_e$ (%)	37.656	28.950
χ^2	0.099	0.129

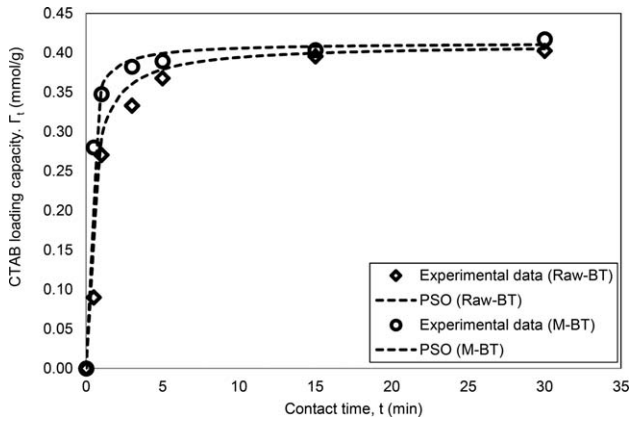

Figure 4. Kinetics of CTAB adsorption onto Raw-BT and M-BT agrosorbents. Experimental conditions: CTAB concentration, 1.0 mmol/L; pH, 7; temperature (30 ± 1)°C; and dosage, 2 mg/mL.

that the CTAB loading for the Raw-BT and M-BT followed the Langmuir model, where monolayer CTAB loading was suggested.

Effects of Surfactant Loading Capacity

The relationship between the surfactant loading capacity, Γ_e and the benzene adsorption capacity, q_e (mmol/g) was studied by preparing agrosorbents with various CTAB concentrations. The M-0.5CTAB-BT, M-2CTAB-BT, M-5CTAB-BT, and M-20CTAB-BT were prepared by reacting M-BT with (0.5, 2.0, 5.0, and 20.0) mmol/L CTAB solutions, respectively. The CTAB loading capacity, Γ_e (mmol/g) was calculated and presented in Figure 6. The adsorption of benzene by four types of M-CTAB-BT shows that their q_e drastically increased from (2 to 5) mmol/L CTAB and remained almost constant above 5 mmol/L of CTAB due to the complete occupancy of the binding sites of the M-BT. The adsorption capacity, Γ_e increased the most between M-2CTAB-BT and M-5CTAB-BT (Figure 6). These results proved that the q_e could be

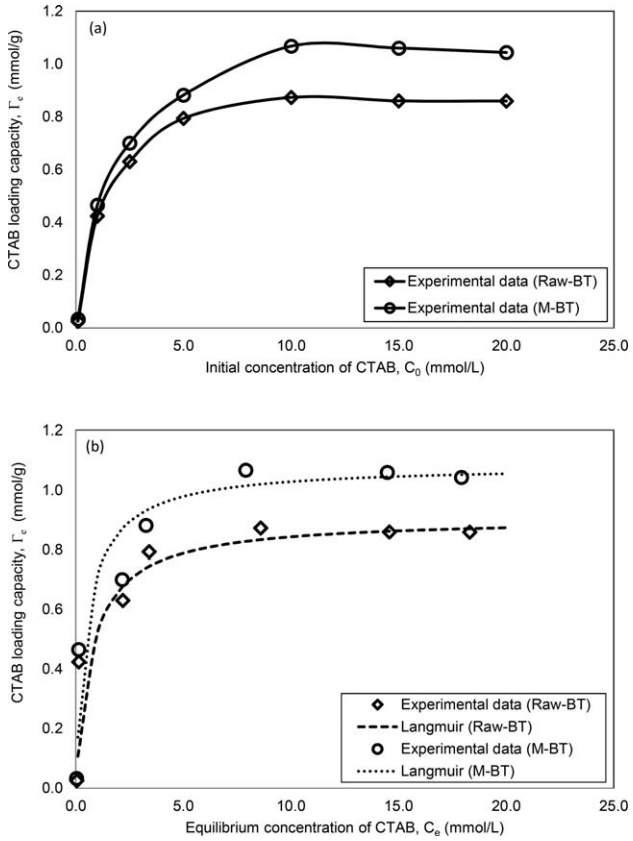

Figure 5. (a) Effect of initial CTAB concentrations on CTAB loading capacity. Experimental conditions: contact time, 2 h; pH, 7; temperature (30 ± 1)°C; and dosage, 2 mg/mL). (b) Isotherm model analysis of CTAB adsorption equilibrium data.

influenced by the CTAB adsorption capacity (Γ_e) on M-BTs where the steepest q_e slope was observed between M-2CTAB-BT (108.048 mmol/g) and M-5CTAB-BT (283.993 mmol/g).

Benzene Adsorption Isotherms

Figure 7a shows that the M-CTAB-BT achieved a higher q_e than the CTAB-BT. This was attributed to the higher CTAB loading capacity of the M-CTAB-BT. The q_e increased when the C_0 increased gradually from (0.1 to 2.5) mmol/L. At low concentration, the q_e was relatively low due to the inadequate quantity of benzene molecules in the solution. When the benzene molecules increased with the initial benzene concentration, the q_e also increased. The benzene adsorption reached the stage in which all the active sites on agrosorbent surfaces were hypothetically fully occupied. This was observed at the benzene concentrations greater than 2.5 mmol/L.

The benzene adsorption equilibrium data of the agrosorbents were further analyzed by the isotherm models: (a) Langmuir; (b) Freundlich; (c) Temkin; and (d) Dubinin–Raduchkevich (D–R) in which the nonlinear and linear equations were given in Supporting Information (SI 2) [68], respectively. The isotherm parameters are tabulated in Table 6, which were generated from the linear fitting of the respective models. The R^2 value had no distinct difference between the Langmuir and Freundlich models, however, the lower Δq_e and χ^2 values of the Langmuir model for Raw-BT, CTAB-BT and M-CTAB-BT suggested the validity of the model. The $q_{e,max,\ L}$ (mmol/g) calculated using the Langmuir equation

Table 5. Isotherm model parameters obtained from CTAB loading capacity analysis.

Samples Parameters	Raw-BT	M-BT
$\Gamma_{e,max,exp}$ (mmol/g)	0.859	1.043
Langmuir		
k_L (L/mmol)	1.335	1.875
$\Gamma_{max,L}$ (mmol/g)	0.907	1.083
R^2	0.992	0.997
$\Delta\Gamma_e$ (%)	22.722	20.952
χ^2	0.082	0.205
Freundlich		
k_F ($L^n mmol^{n-1}/g$)	0.319	0.409
N	2.070	2.151
R^2	0.677	0.752
$\Delta\Gamma_e$ (%)	72.413	80.014
χ^2	2.370	2.782
Temkin		
a (L/g)	62.943	76.036
b_T (kJ/mol)	18.670	16.053
R^2	0.912	0.957
$\Delta\Gamma_e$ (%)	20.263	19.896
χ^2	0.246	0.337
Dubinin–Raduchkevich		
$q_{e,max,\ D-R}$ (mmol/g)	2.147	2.463
E (kJ/mol)	9.129	10.000
R^2	0.735	0.817
$\Delta\Gamma_e$ (%)	91.915	93.214
χ^2	10.210	11.806

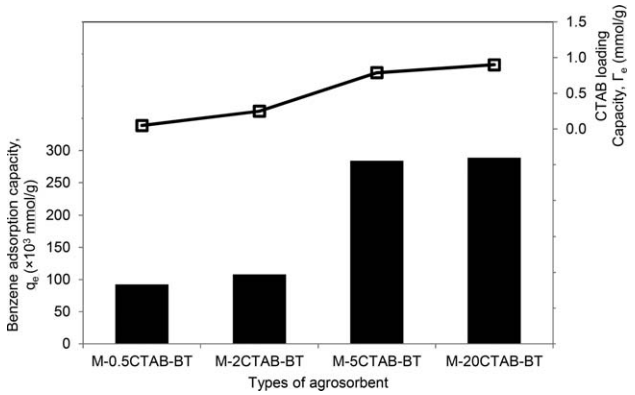

Figure 6. Effects of CTAB loading capacity on benzene adsorption capacity. Experimental conditions: contact time = 24 h; pH, 7; temperature (30 ± 1)°C; and dosage, 2 mg/mL.

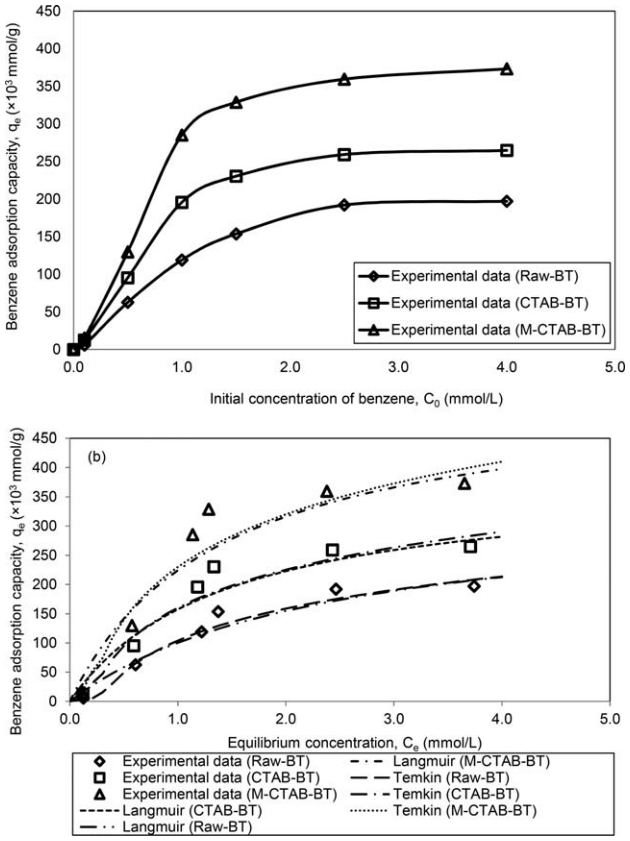

Figure 7. (a) Effect of initial benzene concentrations on benzene adsorption capacity. Experimental conditions: contact time, 24 h; pH, 7; temperature (30 ± 1)°C; and dosage, 0.5 mg/mL. (b) Isotherm model analysis of benzene adsorption equilibrium data.

was relatively close to $q_{e,max,exp}$ (mmol/g) for all experimental data. This confirmed that the benzene adsorption obeyed the Langmuir isotherm model. Apart from that, the mean free energy, E (kJ/mol) analysis of the D–R model was employed to determine the type of adsorption process (i.e., physisorption or chemisorption). It is reported that the chemical ion exchange can occur if E value falls in between (8 and 16) kJ/mol, where the physical and chemical adsorptions can be specified by E value smaller than 8 kJ/mol and E value greater than 16 kJ/mol, respectively [12,69]. The fitting from the D–R model suggested that the benzene adsorption onto agrosorbents was specified as a physical adsorption process because the E value (kJ/mol) fell below 8 kJ/mol. However, the benzene adsorption equilibrium data were found least fitted to D–R models. The heat of adsorption value, b_T decreased with the increasing benzene molecule coverage on the agrosorbent surface (i.e., $q_{e,max,exp}$). Figure 7b shows the fittings of the nonlinear equations (i.e., Langmuir and Temkin) using the isotherm model parameters tabulated in Table 6 because the experimental data could only be well-fitted into these models even though the assumptions might not be completely satisfied. The other model fittings are shown in Supporting Information (SI 5).

Benzene Adsorption Kinetics

The benzene adsorption data at different contact time are given in Figure 8. It was found that the benzene molecules were adsorbed rapidly at the first 500 min then increased gradually for 100 min before achieving equilibrium after 720 min (12 h). The rapid adsorption rate occurred at the initial moment due to the large number of vacant active sites which resulted in greater interactions between agrosorbent active sites and adsorbate molecules. The M-CTAB-BT had the highest benzene adsorption capacity, $q_{t,exp}$ (385.731×10^{-3} mmol/g), followed by the CTAB-BT (242.780×10^{-3} mmol/g) and Raw-BT (193.007×10^3mmol/g). The high $q_{t,exp}$ of the M-CTAB-BT might be caused by its higher CTAB loading capacity.

The time dependency of the benzene adsorption of the agrosorbents could be viewed as a chemical phenomenon in which the data could generally be analyzed by three kinetic models: pseudo-first order (PFO); pseudo-second order (PSO) and Elovich [70]. The mathematical expression of these kinetic models are presented in Supporting Information (SI 1). The kinetic parameters were calculated from the linear

Table 6. Isotherm model parameters obtained from benzene adsorption isotherm analysis.

Samples Parameters	Raw-BT	CTAB-BT	M-CTAB-BT
$q_{e,max,exp}$ ($\times 10^3$mmol/g)	197.108	264.679	373.081
Langmuir			
k_L (L/mmol)	0.417	0.699	0.720
$q_{e,max,L}$ ($\times 10^3$ mmol/g)	340.252	382.409	535.619
R^2	0.927	0.943	0.932
Δq_e (%)	33.562	38.547	38.161
χ^2	0.011	0.018	0.032
Freundlich			
k_F ($L^n mmol^{n-1}/g$)	0.072	0.116	0.161
N	0.944	1.088	1.034
R^2	0.943	0.932	0.921
Δq_e (%)	53.192	49.794	51.728
χ^2	0.096	0.128	0.221
Temkin			
a (L/g)	3.730	5.486	5.866
b_T (kJ/mol)	31.904	26.813	19.388
R^2	0.966	0.934	0.914
Δq_e (%)	44.670	40.321	39.514
χ^2	0.008	0.011	0.018
Dubinin–Raduchkevich			
$q_{e,max,D-R}$ ($\times 10^3$ mmol/g)	1081.940	2315.800	6867.192
E (kJ/mol)	7.911	7.127	6.693
R^2	0.960	0.978	0.977
Δq_e (%)	43.648	46.652	64.983
χ^2	0.017	0.089	0.292

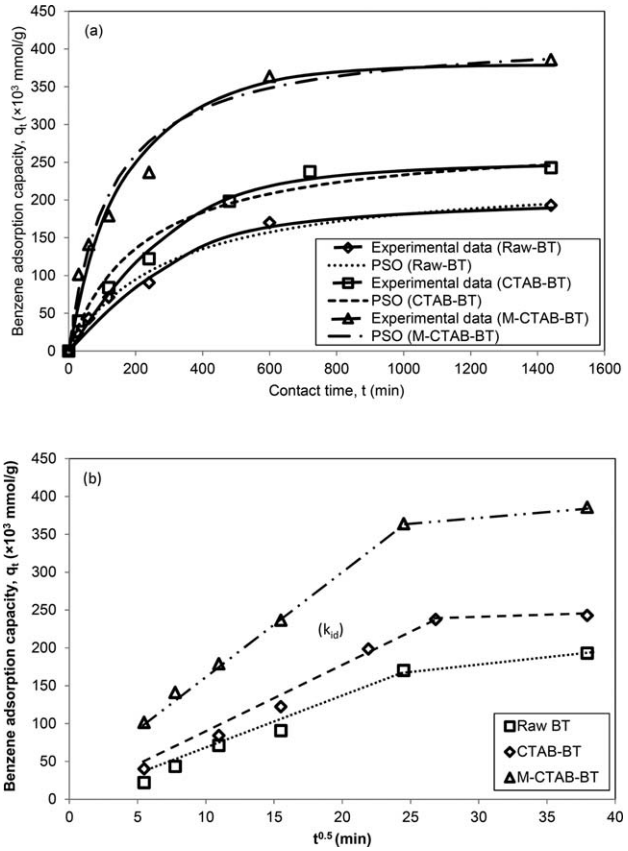

Figure 8. (a) Effect of contact time on benzene adsorption capacity. Experimental conditions: benzene concentration, 1.0 mmol/L; pH, 7; temperature (30 ± 1)°C; and dosage, 0.5 mg/mL. (b) Intraparticle/Weber–Morris plots of benzene adsorption kinetic data.

equation and presented in Table 7. The findings suggest that the benzene adsorption followed the PSO kinetic model. This conclusion was made since the R^2 values obtained from the linear fitting of the Raw-BT, CTAB-BT, and M-CTAB-BT adsorption data into the PSO kinetic model were close to unity (0.990, 0.985, and 0.995, respectively). These R^2 values were relatively higher in comparison with R^2 values given by the PSO and Elovich kinetic models. The Δq_e and χ^2 values obtained for the PSO model were also relatively smaller than other kinetic models (Table 7). In addition, the $q_{t,cal}$ (mmol/g) values from the PSO kinetic model were reasonably similar to the $q_{t,exp}$ (mmol/g). All the findings suggested that the benzene adsorptive removal by the agrosorbents was best fitted by the PSO kinetic model (Figure 8a). The other model fittings are shown in Supporting Information (SI 6).

Apart from the above analysis, the adsorption kinetic data could also be evaluated by the diffusion based models such as the Fick's law, Boyd plot, and Weber–Morris model. The intraparticle diffusion of benzene molecules was examined by employing the Weber and Morris equation (Supporting Information SI 1). The values of k_{id} for Raw-BT, CTAT-BT, and M-CTAB-BT were calculated and tabulated in Table 7. According to the previous study, intraparticle diffusion is the sole rate limiting step if the plot of q_e against $t^{0.5}$ intercepts at the point of zero [71]. Figure 8b demonstrates the intraparticle diffusion plots which did not pass through the origin therefore a two-step multilinear adsorption process was expected. Figure 8b also shows clearly that all the first-linear plots were steeper than the second-linear plots. This indicates that the diffusion of benzene molecules was fast during the first stage and slowed gradually in the second stage [67]. The value of k_{id} (mmol g^{-1} $min^{-0.5}$) increased from Raw-BT (5.517) < CTAB-BT (7.149) < M-CTAB-BT (14.451). This means that the benzene molecules diffused most rapidly into M-CTAB-BT among all three agrosorbents. However, the Weber and Morris equation predicts only the initial insight into the diffusing mechanism. The above discussion suggests obviously that the intraparticle diffusion is not the only rate-limiting step. Thus, in order to confirm the rate-limiting step, the effective diffusion coefficient (D_{eff}) was determined by the Boyd plot [66]. The different q_t/q_e values were obtained for benzene adsorption at different stage (q_t) using the following equations.

$$q_t/q_e > 0.85;\ B_t = -0.4997 - \ln\left(1 - \left[q_t/q_e\right]\right) \quad (3)$$

$$q_t/q_e < 0.85;\ B_t = \left(\sqrt{\pi} - \sqrt{\pi - \left(\frac{\pi^2\left[q_t/q_e\right]}{3}\right)}\right)^2 \quad (4)$$

The q_t/q_e was plotted versus time. The linear Boyd plot gradient (S_{eff}) was utilized to determine effective pore diffusion coefficient, D_{eff} by applying (5)), where 'a' is the agrosorbent particle spherical radius (m). The D_{eff} is actually the summation of pore diffusion and pore surface diffusion coefficients, where the pore surface diffusion coefficient is small and hence can be assumed to be negligible.

$$S_{eff} = \frac{\pi^2 D_{eff}}{a^2} \quad (5)$$

The film diffusion coefficient (D_{film}) was derived from the Fick's law model in which it was obtained from the gradient (S_{film}) of the q_t/q_e against $t^{0.5}$ plot using (6)).

Table 7. Kinetic model parameters obtained from benzene adsorption kinetic analysis.

Parameters/samples		Raw-BT	CTAB-BT	M-CTAB-BT
$q_{t,\ exp}$ ($\times 10^3$ mmol/g)		193.007	242.780	385.731
Chemical reaction based kinetic models	Pseudo-first order			
	$q_{t,\ cal}$ ($\times 10^3$ mmol/g)	204.538	232.701	333.204
	k_1 (min^{-1})	0.003	0.003	0.003
	R^2	0.997	0.962	0.993
	Δq_e (%)	34.086	37.191	41.316
	χ^2	0.006	0.028	0.383
	Pseudo-second order			
	$q_{t,cal}$ ($\times 10^3$ mmol/g)	234.522	284.414	419.815
	k_2 (min^{-1})	0.014	0.016	0.019
	R^2	0.990	0.985	0.995
	Δq_e (%)	34.566	31.477	26.713
	χ^2	0.003	0.008	0.011
	Elovich			
	β (g/mmol)	37.037	28.571	17.857
	α (mmol/g.min)	0.007	0.014	0.026
	R^2	0.811	0.874	0.917
	Δq_e (%)	35.826	29.074	37.160
	χ^2	0.052	0.045	0.037
Diffusion based kinetic models	Weber–Morris			
	k_{id} (mmol g^{-1} $min^{-0.5}$)	5.517	7.149	14.451
	R^2	0.950	0.929	0.993
	Boyd plot			
	D_{eff} ($\times 10^{13}$ m^2/min)	22.435	12.820	12.820
	R^2	0.999	0.966	0.968
	Fick's Law			
	D_{film} ($\times 10^{13}$ m^2/min)	2.165	1.867	1.461
	R^2	0.933	0.921	0.907

$$q_t/_{q_e} = 6\sqrt{\frac{D_{film}}{\pi a^2}} \cdot \sqrt{t} \quad (6)$$

The calculated results indicated that the D_{film} value for Raw-BT, CTAB-BT, and M-CTAB-BT was found to be comparatively smaller than D_{eff} value (Table 7). This indicated that the benzene transfer process was limited in the film boundary. The surface modification was also observed to affect the calculated values of D_{eff} and D_{film} for the agrosorbents, in which the largest value was observed for the Raw-BT followed by CTAB-BT and M-CTAB-BT. This pattern indicated that the Raw-BT has the fastest pore and film diffusion rate in comparison with CTAB-BT and M-CTAB-BT. The low diffusion rate can be attributed to the CTAB loading on to the particular agrosorbent surfaces. The bulky structure (i.e., long tail) of the CTAB might slow down the diffusion rate of benzene onto the surfaces. As previously discussed, the M-CTAB-BT had the lowest surface area and pore diameter among all the agrosorbents due to the higher CTAB loading capacity. This indicated that the CTAB modification did not improve benzene adsorption rate via pore and film diffusion.

Mechanism of Benzene Adsorption

Adsorption involves physical and chemical processes [71]. Generally, low molecular weight aromatic compounds are adsorbed by nonspecific attraction [42]. Benzene adsorption mechanism could be drawn from the isotherm and kinetic data analysis results as previously discussed. The benzene adsorption was a monolayer adsorption since the experimental data were best fitted to the Langmuir model. It was assumed that there were no interactions between the adsorbed benzene molecules. In addition, the benzene adsorption was characterized by a physisorption as the E value of Raw-BT, CTAB-BT, and M-CTAB-BT was (7.911, 7.127, and 6.693) kJ/mol, respectively [72]. However, it should be noted that the present benzene adsorption data were found less fitted in the D–R model. These results were based on the fact that the adsorption was viewed as a chemical phenomenon in which the benzene molecules reacted with the active sites on the agrosorbent surfaces. The benzene adsorption onto agrosorbents could also be viewed as a physical phenomenon as the both adsorption phenomena occurred simultaneously during the adsorption process. The physical phenomenon includes (a) bulk, (b) film, and (c) intraparticle diffusions. As the results shown, the benzene adsorption was rapid at the first few hours observed for all agrosorbents as justified by the Weber and Morris kinetic model analysis, whereby the k_{id} values were greater in the first stage of all adsorption cases. This might attribute to the

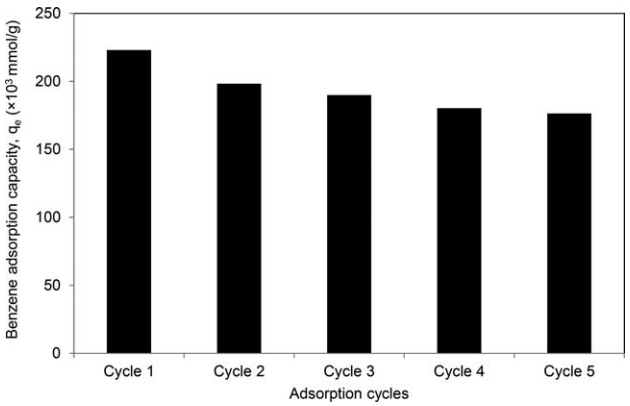

Figure 9. Adsorption performance of M-CTAB-BT as a function of adsorption cycles. Experimental conditions: benzene concentration, 1.0 mmol/L; contact time, 24 h; pH, 7; temperature (30 ± 1)°C; and dosage, 0.5 mg/mL.

Table 8. Benzene adsorption capacity comparison among low-cost agrosorbents.

Agrosorbent	Chemical modification	Adsorption capacity, q ($\times 10^3$mmol/g)	Conditions	Reference
Banana trunk fiber (BT)	Unmodified (Raw-BT)	197.108[E] 340.252[L]	pH 7; T:30 ± 1; C_0: 4.0; S/L: 0.5	Present study
	CTAB loaded (CTAB-BT)	264.679[E] 382.409[L]		
	Mercerized and CTAB loaded. (M-CTAB-BT)	373.081[E] 535.619[L]		
Natural jute	Delignified	340.520[L]	T: 25 ± 1; C_0: 20; S/L: 0.5	[21]
	Treated with palmitic anhydride	501.780[L]		
Cellulose fibre	Grafted with octanoic anhydride	210.000[E]	pH 6.5–7; T: 25; C_0: 0–2.5; S/L: 10	[74]
Angico sawdust	Unmodified	0.028[E]	T: 25 ± 1; C_0: 0.0013; S/L: 7.69	[42]
Peat	Unmodified	0.085[E]		

*Note: [E]Experimental data; [L]Langmuir data; C_0: Initial Concentration (mmol/L); T: Temperature (°C); S/L: agrosorbent dosage (g/mL)

numerous vacant adsorptive sites on agrosorbent surfaces. The benzene adsorption rate decreased gradually with time and it finally achieved equilibrium after 12 h. The Weber–Morris kinetic analysis did not suggest intraparticle diffusion as the sole rate limiting step because the plot did not pass through the origin. The pore diffusion and film diffusion analysis were further conducted to determine the benzene adsorption mechanism. The pore diffusion was found faster than the film diffusion by which it could be concluded that the overall adsorption rate was limited by the film boundary diffusion.

Future Prospects of Agrosorbents

An adsorbent should have good recyclable and reusable characteristics so that it could minimize the operating costs of adsorption process [73]. Organic solvents such as alcohol are commonly used to desorb loaded organic compounds, such as benzene on exhausted agrosorbents. Figure 9 illustrates the benzene adsorption data of the recycled modified banana trunk agrosorbent (M-CTAB-BT) for multiple adsorption cycles. It could be observed vividly that the q_e of M-CTAB-BT decreased gradually from the first cycle (223.122×10^{-3} mmol/g) to the last cycle (176.425×10^{-3} mmol/g). The reduction of q_e throughout the adsorption–desorption cycles could be attributed to the CTAB leaching from the agrosorbent surfaces. In this study, 50% (v/v) of ethanol–water was used as a desorbing solution to desorb benzene molecules from the benzene loaded M-CTAB-BT. It was found that during the first desorption cycle, 0.13 mmol/L CTAB was detected in the desorbing solution followed by (0.07 and 0.01) mmol/L CTAB, respectively in second and third desorption cycles. However, there was no significant CTAB content found in the ethanol–water solution for the fourth and last adsorption–desorption cycles. The CTAB leaching observed in each cycle, correlated well to the extent of q_e. For instance, the most severe q_e reduction (11.2%) was observed for the second adsorption–desorption cycle followed by third (4.1%), fourth (5.1%), and fifth (2.1%) cycles. Figure 9 shows that the repeatedly washed M-CTAB-BT could be reused for five continuous cycles with no drastic q_e loss. Although the q_e of the regenerated M-CTAB-BT declined after multiple adsorption cycles, it was still higher than the adsorption capacity achieved by unmodified or intermediate agrosorbents as shown in Table 3. This finding indicated the advantages of mercerized and surfactant modified agrosorbent compared to the conventional adsorbents including zeolites and activated carbons.

Benzene adsorption performance is significantly related to the characteristics of agrosorbent including the presence of the particular functional groups. Surface mercerization was conducted to increase the amount of carboxyl groups on the agrosorbent surface. Hence, the binding sites of BT surface could be enhanced which led to a higher Γ_e and thus a higher q_e as observed for the M-CTAB-BT. It was proven that benzene adsorption was most favorable to M-CTAB-BT in comparison with the Raw-BT and CTAB-BT due to the smaller value of b_T, which indicated less heat of adsorption is required for the benzene molecules to adsorb on to the M-CTAB-BT surface. Table 8 shows the comparison of benzene adsorption uptake (mmol/g) for several agrosorbents indicating that the M-CTAB-BT gave a relatively better benzene adsorption uptake in comparison to materials such as peat (0.085×10^{-3} mmol/g) and angico sawdust (0.028×10^{-3} mmol/g) [42].

CONCLUSIONS

Agrowaste of banana trunk (BT) was used as a precursor for the CTAB coated agrosorbent (M-CTAB-BT) synthesis through mercerization and surfactant coating processes. This agrosorbent was characterized against the raw BT (Raw-BT), mercerized BT (M-BT) and CTAB coated BT (i.e., CTAB-BT and M-CTAB-BT). The CTAB loading capacity, Γ_e (mmol/g) increased with concentration and by using M-BT. The equilibrium and kinetic data obeyed the Langmuir isotherm and PSO kinetic models. The benzene adsorption capacity, q_e increased with Γ_e. The adsorption data analysis indicated that the benzene adsorption onto Raw-BT, CTAB-BT, and M-CTAB-BT obeyed the Langmuir isotherm and PSO kinetic models. In addition, it was revealed that the benzene adsorption was dominated by the film boundary diffusion as the rate-limiting step. These results thus suggested that agrowaste such as the modified BT could potentially be employed as agrosorbent precursors for various organic pollutants such as BTEX removal from the waste waters through appropriate modifications such as mercerization and surfactant modification to enhance their adsorption equilibrium and kinetics.

ACKNOWLEDGEMENTS

The financial supports of the Research University Grant from Universiti Teknologi Malaysia (GUP Grant Nos. 00H63

and 06H85), the PhD scholarship from Universiti Teknologi Malaysia and Universiti Teknologi Malaysia Post Doctoral Fellowship Scheme awarded to Norasikin Saman are gratefully acknowledged.

Literature Cited

1. Vidal, C.B., Raulino, G.S.C., Barros, A.L., Lima, A.C.A., Ribeiro, J.P., Pires, M.J.R., & Nascimento, R.F. (2012). BTEX removal from aqueous solutions by HDTMA-modified Y zeolite, Journal of Environmental Management, 112, 178–185.
2. Kim, S.-H., Park, J.-H., Hong, Y., & Lee, C.-Y. (2014). Removal of BTX using granular octyl-functionalized mesoporous silica nanoparticle, International Biodeterioration and Biodegradation, 95, 219–224.
3. Torabian, A., Kazemian, H., Seifi, L., Bidhendi, G.N., Azimi, A.A., & Ghadiri, S.K. (2010). Removal of petroleum aromatic hydrocarbons by surfactant-modified natural zeolite: The effect of surfactant, Clean Soil, Air, Water, 38, 77–83.
4. Asenjo, N.G., Álvarez, P., Granda, M., Blanco, C., Santamaría, R., & Menéndez, R. (2011). High Performance activated carbon for benzene/toluene adsorption from industrial wastewater, Journal of Hazardous Materials, 192, 1525–1532.
5. Aivalioti, M., Papoulias, P., Kousaiti, A., & Gidarakos, E. (2012). Adsorption of BTEX, MTBE and TAME on natural and modified diatomite, Journal of Hazardous Materials, 207–208, 117–127.
6. Chung, E.K., Jang, J.K., & Koh, D.H. (2016). A comparison of benzene exposures in maintenance and regular works at Korean petrochemical plants, Journal of Chemical Health and Saftey, 24, 21–26.
7. Moro, A.M., Brucker, N., Charão, M.F., Baierle, M., Sauer, E., Goethel, G., … Garcia, S.C. (2017). Biomonitoring of gasoline station attendants exposed to benzene: Effect of gender, Mutation Research: Toxicology and Environmental Mutagen, 813, 1–9.
8. Gupta, A.K., & Ahmad, M. (2011). Study of the effect of refinery waste water exposure on Allium cepa's enzymatic antioxidant defense: Probing potential biomarkers, Toxicology and Environmental Chemistry, 93, 1166–1179.
9. Chiriac, R., Carré, J., Perrodin, Y., Vaillant, H., Gasso, S., & Miele, P. (2009). Study of the Dispersion of VOCs emitted by a municipal solid waste landfill, Atmosphere and Environment, 43, 1926–1931.
10. Su, F., Lu, C., & Hu, S. (2010). Adsorption of benzene, toluene, ethylbenzene and *p*-xylene by NaOCl-oxidized carbon nanotubes, Colloids Surfaces A: Physicochemical Engineering Aspects, 353, 83–91.
11. Carvalho, M.N., da Motta, M., Benachour, M., Sales, D.C.S., Abreu, C.A.M., Motta, M., … Abreu, C.A.M. (2012). Evaluation of BTEX and phenol removal from aqueous solution by multi-solute adsorption onto smectite organoclay, Journal of Hazardous Materials, 239–240, 95–101.
12. Nourmoradi, H., Nikaeen, M., Khiadani, H.H., & Hajian, M.K. (2012). Removal of benzene, toluene, ethylbenzene and xylene (BTEX) from aqueous solutions by montmorillonite modified with nonionic surfactant: Equilibrium, kinetic and thermodynamic study, Chemical Engineering Journal, 191, 341–348.
13. Moura, C.P., Vidal, C.B., Barros, A.L., Costa, L.S., Vasconcellos, L.C.G., Dias, F.S., & Nascimento, R.F. (2011). Adsorption of BTX (benzene, toluene, *o*-xylene, and *p*-xylene) from aqueous solutions by modified periodic mesoporous organosilica, Journal of Colloid and Interface Science, 363, 626–634.
14. Hiwarkar, A.D., Srivastava, V.C., & Deo mall, I. (2015). Comparative studies on adsorptive removal of indole by granular activated carbon and bagasse fly ash, Environmental Progress and Sustainable Energy, 34, 492–503.
15. Zytner, R.G. (1994). Sorption of benzene, toluene, ethylbenzene and xylenes to various media, Journal of Hazardous Materials, 38, 113–126.
16. Liang, C., & Chen, Y.-J. (2010). Evaluation of activated carbon for remediating benzene contamination: adsorption and oxidative regeneration, Journal of Hazardous Materials, 182, 544–551.
17. Mohammed, J., Nasri, N.S., Ahmad Zaini, M.A., Hamza, U.D., & Ani, F.N. (2015). Adsorption of benzene and toluene onto KOH activated coconut shell based carbon treated with NH3, International Biodeterioration and Biodegradation, 102, 245–255.
18. Wibowo, N., Setyadhi, L., Wibowo, D., Setiawan, J., & Ismadji, S. (2007). Adsorption of benzene and toluene from aqueous solutions onto activated carbon and its acid and heat treated forms: Influence of surface chemistry on adsorption, Journal of Hazardous Materials, 146, 237–242.
19. Yakout, S.M., & Daifullah, A.A.M. (2013). Adsorption/desorption of BTEX on activated carbon prepared from rice husk, Desalination & Water Treatment, 52, 4485–4491.
20. Hindarso, H., Ismadji, S., Wicaksana, F., & Indraswati, N. (2001). Adsorption of benzene and toluene from aqueous solution onto granular activated carbon, Journal of Chemical Engineering and Data Mining, 46, 788–791.
21. Serrano, L., Urruzola, I., Nemeth, D., Bela, K., & Labidi, J. (2011). Modified cellulose microfibrils as benzene adsorbent, Desalination, 270, 143–150.
22. Daifullah, A.A.M., & Girgis, B.S. (2003). Impact of surface characteristics of activated carbon on adsorption of BTEX, Colloids and Surfaces A: Physicochemical and Engineering Aspects, 214, 181–193.
23. Koyuncu, H., Yıldız, N., Salgın, U., Köroğlu, F., & Calımlı, A. (2011). Adsorption of *o*-, *m*- and *p*-nitrophenols onto organically modified bentonites, Journal of Hazardous Materials, 185, 1332–1339.
24. Lu, C., Su, F., & Hu, S. (2008). Surface modification of carbon nanotubes for enhancing BTEX adsorption from aqueous solutions, Applied Surface Science, 254, 7035–7041.
25. Su, F., Lu, C., Johnston, K. R., & Hu, S. (2010). Kinetics, thermodynamics, and regeneration of BTEX adsorption in aqueous solutions via NaOCl-oxidized carbon nanotubes. In Environanotechnology (1st Edition) (pp. 71–97), Amsterdam: Elsevier.
26. Yu, F., Wu, Y., Li, X., & Ma, J. (2012). Kinetic and thermodynamic studies of toluene, ethylbenzene, and *m*-xylene adsorption from aqueous solutions onto KOH-activated multiwalled carbon nanotubes, Journal of Agricultural Food Chemistry, 60, 12245–12253.
27. Seifi, L., Torabian, A., Kazemian, H., Bidhendi, G.N., Azimi, A.A., Farhadi, F., & Nazmara, S. (2011). Kinetic study of BTEX removal using granulated surfactant-modified natural zeolites nanoparticles, Water Air Soil Pollution, 219, 443–457.
28. Ghiaci, M., Abbaspur, A., Kia, R., & Seyedeyn-Azad, F. (2004). Equilibrium isotherm studies for the sorption of benzene, toluene, and phenol onto organo-zeolites and as-synthesized MCM-41, Separation and Purification Technology, 40, 217–229.
29. Jaynes, W.F., & Vance, G.F. (1999). Sorption of benzene, toluene, ethylbenzene, and xylene (BTEX) compounds by hectorite clays exchange with aromatic organic cations, Clays and Clay Minerals, 47, 358–365.

30. Vianna, M.M.G.R., Valenzuela-Díaz, F.R., Kozievitch, V.F.J., Dweck, J., & Büchler, P.M. (2005). Synthesis and characterization of modified clays as sorbents of toluene and xylene, Material Science Forum, 498–499, 691–696.
31. Sharmasarkar, S., Jaynes, W.F., & Vance, G.F. (2000). BTEX sorption by montmorillonite organo-clays: TMPA, ADAM, HDTMA, Water, Air, Soil Pollution, 119, 257–273.
32. Lin, S.H., & Huang, C.Y. (1999). Adsorption of BTEX from aqueous solution by macroreticular resins, Journal of Hazardous Materials, 70, 21–37.
33. Aivalioti, M., Vamvasakis, I., & Gidarakos, E. (2010). BTEX and MTBE adsorption onto raw and thermally modified diatomite, Journal of Hazardous Materials, 178, 136–143.
34. Dou, B., Li, J., Wang, Y., Wang, H., Ma, C., & Hao, Z. (2011). Adsorption and desorption performance of benzene over hierarchically structured carbon-silica aerogel composites, Journal of Hazardous Materials, 196, 194–200.
35. Uragami, T., Fukuyama, E., & Miyata, T. (2016). Selective removal of dilute benzene from water by poly(methyl methacrylate)-graft-poly(dimethylsiloxane) membranes containing hydrophobic ionic liquid by pervaporation, Journal of Membrane Science, 510, 131–140.
36. Mukherjee, R., & De, S. (2016). Novel carbon-nanoparticle polysulfone hollow fiber mixed matrix ultrafiltration membrane: Adsorptive removal of benzene, phenol and toluene from aqueous solution, Separation and Purification Technology, 157, 229–240.
37. Ohshima, T., Miyata, T., & Uragami, T. (2005). Selective removal of dilute benzene from water by various cross-linked poly(dimethylsiloxane) membranes containing tert-butylcalix[4]arene, Macromolecular Chemistry and Physics, 206, 2521–2529.
38. Ong, Y.T., Ahmad, A.L., Zein, S.H.S., & Tan, S.H. (2010). A review on carbon nanotubes in an environmental protection and green engineering perspective, Brazilian Journal of Chemical Engineering, 27, 227–242.
39. Kasuriya, S., Namuangruk, S., Treesukol, P., Tirtowidjojo, M., & Limtrakul, J. (2003). Adsorption of ethylene, benzene, and ethylbenzene over faujasite zeolites investigated by the ONIOM method, Journal of Catalysis, 219, 320–328.
40. Xie, J., Meng, W., Wu, D., Zhang, Z., & Kong, H. (2012). Removal of organic pollutants by surfactant modified zeolite: Comparison between ionizable phenolic compounds and non-ionizable organic compounds, Journal of Hazardous Materials, 231–232, 57–63.
41. Adachi, A., Ikeda, C., Takagi, S., Fukao, N., Yoshie, E., & Okano, T. (2001). Efficiency of rice bran for removal of organochlorine compounds and benzene from industrial wastewater, Journal of Agricultural Food Chemistry, 49, 1309–1314.
42. Costa, A.S., Romão, L.P.C., Araújo, B.R., Lucas, S.C.O., Maciel, S.T.A., Wisniewski, A., & Alexandre, M.R. (2012). Environmental strategies to remove volatile aromatic fractions (BTEX) from petroleum industry wastewater using biomass, Bioresource Technology, 105, 31–39.
43. Akhtar, M., Bhanger, M. I., Iqbal, S., & Hasany, S. M. (2005). Efficiency of rice bran for the removal of selected organics from water: Kinetic and thermodynamic investigations, Journal of Agricultural Food Chemistry, 53, 8655–8662.
44. Johari, K., Saman, N., Song, S.T., Chin, C.S., Kong, H., & Mat, H. (2016). Adsorption enhancement of elemental mercury by various surface modified coconut husk as eco-friendly low-cost adsorbents, International Biodeterioration and Biodegradation, 109, 45–52.
45. Ibrahim, S., Fatimah, I., Ang, H.-M., & Wang, S. (2010). Adsorption of anionic dyes in aqueous solution using chemically modified barley straw, Water Science and Technology, 62, 1177–1182.
46. Fu, F., & Wang, Q. (2011). Removal of heavy metal ions from wastewaters: A review, Journal of Environmental Management, 92, 407–418.
47. Delval, F., Crini, G., Bertini, S., Filiatre, C., & Torri, G. (2005). Preparation, characterization and sorption properties of crosslinked starch-based exchangers, Carbohydrate Polymers, 60, 67–75.
48. Akhtar, M., Moosa Hasany, S., Bhanger, M.I., & Iqbal, S. (2007). Sorption potential of *Moringa oleifera* pods for the removal of organic pollutants from aqueous solutions, Journal of Hazardous Materials, 141, 546–556.
49. Hashim, M.Y., Roslan, M.N., Amin, A.M., Ahmad Zaidi, A.M., & Ariffin, S. (2012). Mercerization treatment parameter effect on natural fiber reinforced polymer matrix composite: A brief review, World Academic Science of Engineering and Technology, 68, 1638–1644.
50. Koay, Y.S., Ahamad, I.S., Nourouzi, M.M., Abdullah, L.C., & Choong, T.S.Y. (2014). Development of novel low-cost quaternized adsorbent from palm oil agriculture waste for reactive dye removal, Bioresources, 9, 66–85.
51. Foo, K.Y., & Hameed, B.H. (2012). Microporous and mesoporous materials porous structure and adsorptive properties of pineapple peel based activated carbons prepared via microwave assisted KOH and K2CO3 activation, Microporous and Mesoporous Materials, 148, 191–195.
52. Shin, E.W., & Rowell, R.M. (2005). Cadmium ion sorption onto lignocellulosic biosorbent modified by sulfonation: The origin of sorption capacity improvement, Chemosphere, 60, 1054–1061.
53. Chakraborty, S., Sahoo, B., Teraoka, I., Miller, L.M., & Gross, R.A. (2005). Enzyme-catalyzed regioselective modification of starch nanoparticles, Macromolecules, 38, 61–68.
54. Teli, M.D., & Valia, S.P. (2013). Acetylation of banana fibre to improve oil absorbency, Carbohydrate Polymers, 92, 328–333.
55. Alila, S., & Boufi, S. (2009). Removal of organic pollutants from water by modified cellulose fibres, Industrial Crops and Products, 30, 93–104.
56. Paria, S., & Khilar, K.C. (2004). A review on experimental studies of surfactant adsorption at the hydrophilic solid–water interface, Advances in Colloid and Interface Science, 110, 75–95.
57. Ibrahim, S., Ang, H.M., & Wang, S. (2009). Removal of emulsified food and mineral oils from wastewater using surfactant modified barley straw, Bioresource Technology, 100, 5744–5749.
58. Namasivayam, C., & Sureshkumar, M.V. (2008). Removal of chromium(VI) from water and wastewater using surfactant modified coconut coir pith as a biosorbent, Bioresource Technology, 99, 2218–2225.
59. Zhao, B., Xiao, W., Shang, Y., Zhu, H., & Han, R. (2014). Adsorption behavior of light green anionic dye using cationic wheat straw in batch and column mode, Environmental Science and Pollution Research, 20, 5558–5568.
60. Zhang, R., Zhang, J., Zhang, X., Dou, C., & Han, R. (2014). Adsorption of Congo Red from aqueous solutions using cationic surfactant modified wheat straw in batch mode: Kinetic and equilibrium study, Journal of Taiwan Institute of Chemical Engineering, 45, 2578–2583.
61. Bingol, A., Ucun, H., Bayhan, Y.K., Karagunduz, A., Cakici, A., & Keskinler, B. (2004). Removal of chromate anions from aqueous stream by a cationic surfactant-modified yeast, Bioresource Technology, 94, 245–249.

62. Koh, S.M., & Dixon, J.B. (2001). Preparation and application of organo-minerals as sorbents of phenol, benzene and toluene, Applied Clay Science, 18, 111–122.
63. Kong, H., Cheu, S.-C., Othman, N.S., Song, S.-T., Saman, N., Johari, K., & Mat, H. (2016). Surfactant modification of banana trunk as low-cost adsorbents and their high benzene adsorptive removal performance from aqueous solution, RSC Advances, 6, 24738–24751.
64. Cui, L., Puerto, M., Lo, J.L., Biswal, S.L., & Hirasaki, G.J. (2014). Improved methylene blue two-phase titration method for determining cationic surfactant concentration in high-salinity brine, Analytical Chemistry, 86, 11055–11061.
65. Lee, S.Y., Kim, S.J., Chung, S.Y., & Jeong, C.H. (2004). Sorption of hydrophobic organic compounds onto organoclays, Chemosphere, 55, 781–785.
66. Song, S.T., Saman, N., Johari, K., & Mat, H. (2013). Removal of Hg (II) from aqueous solution by adsorption using raw and chemically modified rice straw as novel adsorbents, Industrial & Engineering Chemistry Research, 52, 13092–13101.
67. Saman, N., Johari, K., Song, S.T., & Mat, H. (2014). Removal of Hg(II) and CH3 Hg(I) using rasped pith sago residue biosorbent, CLEAN Soil, Air, Water, 42, 1541–1548.
68. Febrianto, J., Kosasih, A.N., Sunarso, J., Ju, Y.H., Indraswati, N., & Ismadji, S. (2009). Equilibrium and kinetic studies in adsorption of heavy metals using biosorbent: A summary of recent studies, Journal of Hazardous Materials, 162, 616–645.
69. Johari, K., Saman, N., Song, S.T., Mat, H., & Stuckey, D.C. (2013). Utilization of coconut milk processing waste as a low-cost mercury sorbent, Industrial & Engineering Chemistry Research, 52, 15648–15657.
70. Miodrag Belosevic, M. G. E. D. Z. S. J. R. B. (2014). Degradation of Alizarin Yellow R using UV/H_2O_2 advanced oxidation process, Environmental Science and Technology, 33, 482–489.
71. Ho, Y.S., Ng, J. C.Y., & McKay, G. (2000). Kinetics of pollutant sorption by biosorbents: Review, Separation and Purification Reviews, 29, 189–232.
72. Cestari, A.R., Vieira, E.F.S., Vieira, G.S., & Almeida, L.E. (2007). Aggregation and adsorption of reactive dyes in the presence of an anionic surfactant on mesoporous aminopropyl silica, Journal of Colloid and Interface Science, 309, 402–411.
73. Boufi, S., & Belgacem, M.N. (2006). Modified cellulose fibres for adsorption of dissolved organic solutes, Cellulose, 13, 81–94.
74. Aloulou, F., Boufi, S., & Labidi, J. (2006). Modified cellulose fibres for adsorption of organic compound in aqueous solution, Separation and Purification Technology, 52, 332–342.